Journal of Power Sources 199 (2012) 379–385

Contents lists available at SciVerse ScienceDirect

Journal of Power Sources

journal homepage: www.elsevier.com/locate/jpowsour

Spectroscopic and electrochemical characteristics of a carboxylated graphene–ZnO composites

Kyeong-Won Park*, Jong Hwa Jung

Department of Chemistry and Research Institute of Natural Science, Gyeongsang National University, Jinju 660-701, Republic of Korea

ARTICLE INFO

Article history:
Received 28 June 2011
Received in revised form 5 October 2011
Accepted 6 October 2011
Available online 14 October 2011

Keywords:
Carboxylated graphene
Graphene–zinc oxide composite
Graphene oxide
Electrochemical capacitor
Zinc oxide
CV

ABSTRACT

Carboxylated graphene–ZnO (G-COOZn) composites were grown as ZnO nanoparticles onto graphene sheets by a one-step thermal method using carboxylated graphene (G-COOH) and $Zn(NO_3)_2$. G-COOH sheets were synthesized from graphene oxide (GO) and chloroacetic acid ($Cl–CH_2–COOH$). GO was used as the starting material, as prepared by the Hummers' method using graphite flakes. GO, G-COOH, and G-COOZn were characterized by XRD, AFM, SEM, TEM, FT-IR, ^{13}C-NMR, and Raman spectroscopy. The electrochemical properties of the G-COOZn supercapacitor were investigated by cyclic voltammetry, electrochemical impedance spectroscopy, and galvanostatic charge–discharge tests. The results show that the asymmetric supercapacitor has electrochemical capacitance performance within the potential range of 0–1 V. The supercapacitor delivered a specific capacitance of ~238 $F g^{-1}$ at a current density of 50 $mA cm^{-2}$. This method provides an easy and straightforward approach to deposit ZnO nanoparticles onto graphene sheets, and may be readily extended to the preparation of other classes of hybrids based on GO sheets for specific technological applications.

1. Introduction.

Recent research on graphene has focused on a great diversity of technological applications, including nanoelectronic and optoelectronic devices [1–4] as well as energy-storage materials [5–7]. Graphene sheets have an unrolled 2D structure [8,9] and represent a unique morphology carbon material with potential for electrochemical energy storage device applications due to its superb chemical stability [9], high electrical conductivity [10,11], and large surface area [11,12]. The graphene sheets overlap with each other to afford a three-dimensional conducting network, which facilitates electron transfer between the active materials and the charge collector; thus it is an excellent candidate for use as an electrode material for energy-conversion storage systems. Boosting the capacitive performance of graphene-based energy storage materials by growing redox-active materials on the electrically conducting graphene sheets has thus become a topic of major interest. In most graphene-based composites, prepared by reduction of graphene oxide (GO) followed by the loading of pseudocapacitive nanomaterials, the excellent electric and surface properties of the graphene sheets are not completely revealed due to the formation of agglomerations of graphene during the reaction steps. Thu, the seeking of effective strategies to synthesize well-dispersed graphene-based composites remains an important goal.

The use of GO as a material for the preparation of individual graphene sheets in bulk-quantities, has attracted great attention in recent years [13–15]. In addition, the extremely large specific surface area, the abundant oxygen-containing surface functionalities (including epoxide, hydroxyl, carbonyl, and carboxylic groups) and the high water compatibility, all result in GO sheets being of great promise for future applications [13,14]. For instance, GO sheets modified with polyethylene glycol have been employed as aqueous compatible carriers for water-insoluble drug delivery [16]. The oxygen-containing functional groups on GO sheets have been used as sites for the deposition of metal nanoparticles and organic macromolecules, including porphyrins [17,18]. This has opened up a novel route to a range of multifunctional-nanometer scaled catalytic, magnetic, and optoelectronic materials [19–21]. GO sheets, with their distinctive nanostructure hold great promise for potential applications in many technological fields that include nanoelectronics [22], sensors [23], nanocomposites [24], batteries [25], and capacitors [26].

It is known that the presence of metal oxides such as ZnO, MnO_2, IrO_2, RuO_2 and NiO can improve the capacitance of carbon based supercapacitors, as they can contribute additional pseudocapacitance to the capacitance due to arising from the carbon materials [27–30]. It is well known that Zinc oxide, has found applications in optics, optoelectronics, sensors, and actuators due to its semiconducting, piezoelectric, and pyroelectric properties [31]. Recently, the suitability of ZnO as a potential candidate for supercapacitor applications has been preliminarily substantiated [32,33]. Attempts to combine ZnO and graphene have been reported in

* Corresponding author. Tel.: +82 55 772 2634; fax: +82 55 758 6027.
E-mail address: nano2k@nate.com (K.-W. Park).

0378-7753/$ – see front matter © 2011 Elsevier B.V. All rights reserved.
doi:10.1016/j.jpowsour.2011.10.016

efforts to obtain hybrid materials with superior optical or electrical properties [34,35]. Taking into account its eco-friendly nature and the easy growth of wurtzite-structured ZnO on the various substrates, it is meaningful to seek effective preparation strategies and applications of ZnO/GO composites for supercapacitors.

The successful use of –COOH groups combined with Zn (–COOZn) has been previously reported [36–38]. We treated a GO sample with chloroacetic acid under strongly basic conditions in order to activate the epoxide and ester groups, and to convert hydroxyl groups to carboxylic acid (–COOH) moieties [39,40]. The carboxylate groups produced under strongly basic conditions were anticipated to act as a binding site for Zn ion.

In this paper, we report a facile one-pot solvothermal method for the synthesis of a G-COOZn composites using G-COOH and $Zn(NO_3)_2$ as the precursors for forming G-COOZn. The electrochemical properties of G-COOZn were also investigated.

2. Experimental methods

2.1. Preparation of GO

The GO was prepared according to modified Hummers' method [41,42] by reacting commercial flake graphite powder (Aldrich) (5 g) and $NaNO_3$ (3.75 g) with conc. H_2SO_4 (375 mL). This mixture was stirred in an ice-water bath, and 22.5 g of $KMnO_4$ was slowly added over 1 h as stirring was continued for 2 h in an ice-water bath. After the mixture was stirred vigorously for 2 days at room temperature, 700 mL of 5 wt% H_2SO_4 aqueous solution was added over 1 h with stirring, and the temperature was kept at 98 °C. The resultant mixture was further stirred for 2 h at 98 °C. After the temperature was reduced to 60 °C, 15 mL of H_2O_2 (30 wt% aqueous solutions) was added, and the mixture was stirred for 2 h at room temperature. To remove extraneous products from the oxidation (and any other inorganic impurities), the resultant mixture was purified by repeating the following procedure 20 times: centrifugation, removal of the supernatant liquid, then dispersing the solid using vigorous stirring and bath ultrasonication for 1 h at a power of 150 W. The resultant solid was recovered by centrifugation, washed with deionized water and ethanol until H^+ free, and then dried in air at 40 °C.

2.2. Carboxylation of GO

For carboxylation, an aqueous suspension (5 mL) of GO was diluted by a factor of 2 to give a concentration of ~2 mg mL^{-1}, and then bath sonicated for 1 h to give a clear solution. NaOH (1.2 g) and chloroacetic acid (Cl–CH_2–COOH) (1.0 g) were added to the GO suspension and bath sonicated for 2 h to convert the –OH groups to –COOH via conjugation of acetic acid moieties giving G-COOH [39,40]. The resulting G-COOH solution was neutralized, and purified by repeated rinsing and filtration.

2.3. Preparation of G-COOZn composites

The G-COOZn composites were synthesized by a hydrothermal process. In a typical synthesis, G-COOH (0.5 g) and $Zn(NO_3)_2$ (1.00 g) were dispersed in deionized water (20 mL) with ultrasonication for 20 min. Subsequently, the mixture was transferred to a polytetrafluoroethylene-lined autoclave and heated at 180 °C for 10 h. After cooling to room temperature, the resulting gray-black suspension was filtered through a 0.22 μm microporous membrane in order to separate the G-COOZn composites.

2.4. Characterization of GO, G-COOH and G-COOZn composites

The powder X-ray diffraction (XRD) pattern measurements of the samples were recorded on a Bruker D8-Advance X-ray powder diffractometer using Cu Kα radiation (λ = 0.1542 nm) with scattering angles (2θ) of 5–80°, operating at 40 keV, and a cathode current of 20 mA. Scanning electron micrographs (SEM) were obtained using a JEOL JSM-840A scanning electron microscope. Transmission electron micrographs (TEM) were obtained with a JEOL JEM-200 CX transmission electron microscope operating at 200 kV. Atomic force microscopy (AFM) images were obtained using an Auto-Probe CP/MT scanning probe microscope (XE-100(PSIA)). Imaging was carried out in non-contact mode using a V-shaped 'Ultralever' probe B (Park Scientific Instruments, boron doped Si with frequency f_c = 78.6 kHz, spring constants k = 2.0–3.8 Nm^{-1}, and nominal tip radius 10 nm). All images were collected under ambient conditions at 50% relative humidity and 23 °C with a scanning raster rate of 1 Hz. Samples for AFM images were prepared by depositing dispersions of GO in ethanol on a freshly cleaved mica surface (Ted Pella Inc. Prod No. 50) and allowing them to dry in air. Raman spectra were obtained using a Jobin Yvon/Horiba LabRAM spectrometer equipped with an integral microscope (Olympus BX 41). A 514.5 nm Ar-laser was used as an excitation source. Samples were sonicated in ethanol and drops were applied to a glass slide for observation. The sample was viewed using a green laser apparatus under a maximum magnification of ×50, and a red laser apparatus under a magnification of ×100. Solid-state ^{13}C-cross-polarization magic angle spinning nuclear magnetic resonance spectroscopy (^{13}C-NMR) experiments were performed on a 400 MHz Solid-state Bruker Avance II+ spectrometer (at KBSI Daegu Center, KOREA). The Fourier transform infrared (FT-IR) spectra were recorded on a Bruker VERTEX 80v model using the KBr disk method. Steady state photoluminescence (PL) spectra were recorded at room temperature using a Shimadzu RF-5301PC spectrofluorometer.

2.5. Preparation of working electrode and electrochemical tests

The electrochemical measurements were performed in a three-electrode cell system with 1 M Na_2SO_4 aqueous solution as electrolyte. The working electrodes were fabricated by mixing the electroactive materials (G-COOZn), carbon-black, and polytetrafluoroethylene (PTFE) in a mass ratio of 70:20:10 and dispersed in tetrahydrofuran to produce homogeneous slurry. The resulting slurry was coated onto the nickel foam current collector (1 cm × 1 cm) using a blade. And then, the electrodes dried at 70 °C for 12 h. The loading mass of each electrode was about 21.0 mg. Platinum wire and Ag/AgCl (KCl-saturated) electrode were used as counter electrode and reference electrode, respectively. Cyclic voltammetry (CV), galvanostatic charge–discharge, and electrochemical impedance spectroscopy (EIS) were carried out on a PARSTAT 2263 (Princeton Applied Research, USA) instrument. Impedance spectroscopy measurements were performed at a DC bias of 50 mV with sinusoidal signal of 0.1 mV over the frequency range from 10 kHz to 0.1 Hz.

3. Results and discussion

The GO was prepared from flake graphite via a modified Hummers' method [41,42], G-COOH was obtained by reacting GO with chloroacetic acid and the G-COOZn composites were prepared from G-COOH and $Zn(NO_3)_2$. The surface morphology and structure of the as-prepared samples were analyzed by SEM and TEM.

Fig. 1 shows the SEM and TEM results for GO, G-COOH, and G-COOZn. Compared to GO (Fig. 1(a)), the general structure of G-COOH (Fig. 1(b)) is greatly changed. It is found that the jeep-shaped GO

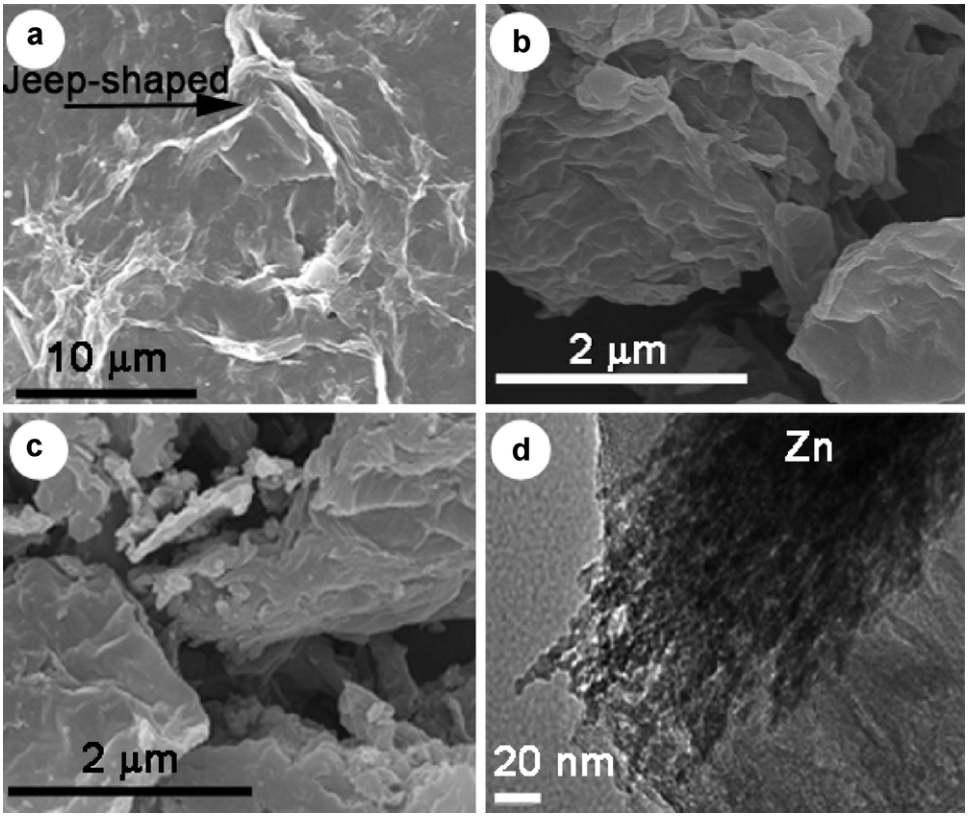

Fig. 1. SEM images of (a) GO, (b) G-COOH, (c) G-COOZn, and (d) TEM image of G-COOZn.

thin plates are well exfoliated. The G has been exfoliated with one sheet so that the jeep-shaped G could be confirmed (Fig. 1(a)). G-COOH was transformed into a wrinkled appearance of one sheet that was evident (Fig. 1(b)). ZnO nanoparticles were observed on the surface of G-COOH (Fig. 1(c) and (d)).

The chemical composition of the G-COOZn sample was analyzed by an energy dispersive spectrometer (EDS) spectrum on an SEM (Fig. 2(a)) that concludes the G-COOZn sample consists of only Zn and O, hence confirming the chemical purity of the sample. The peak corresponding to Au in the EDS spectrum arises from the Au coating used for preparing the SEM specimen. Individual Zn maps are shown in Fig. 2(b). In inset (a) of Fig. 2 we present the EDS mapping of the G-COOZn sample for Zn elements. The mapping of Zn correlates (Fig. 2(b)) well with the remaining red parts in the mapping of G-COOZn. (For interpretation of the references to colour in this text, the reader is referred to the web version of this article.)

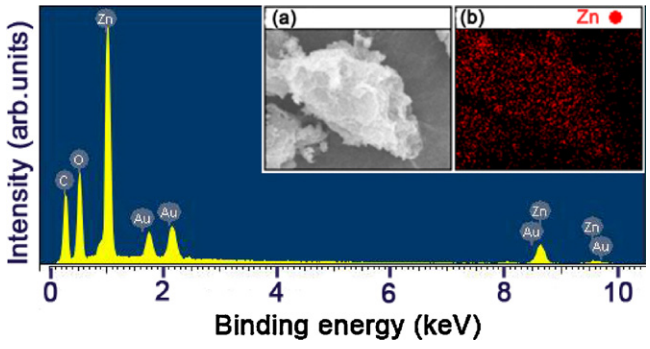

Fig. 2. The EDS spectrum of G-COOZn. Insert (a) SEM images of G-COOZn, and (b) mapping of ZnO linked G-COOH.

The crystalline structures of ZnO nanoparticles on G-COOH were corroborated by XRD measurements. The XRD patterns shown in Fig. 3 reveal that the (*C1 1 0*) diffraction peak of graphite (Fig. 3(a)) appears at 26.8°, which means the interlay space is 0.34 nm. After the exfoliation, the interlay space of the resulting GO (Fig. 3(b); 10.1°, 0.87 nm) became greater than that of graphite due to the introduction of oxygenated functional groups on the graphene sheets [43–45]. The XRD patterns for G-COOH (Fig. 3(c)) commonly exhibit the main peaks at 25.05° and 44.32°. The XRD peaks of the G-COOZn composites were indexed to hexagonal ZnO (JCPDS 36-1451). As shown in Fig. 3(d), the peaks at 31.4°, 34.4°, 36.3°,

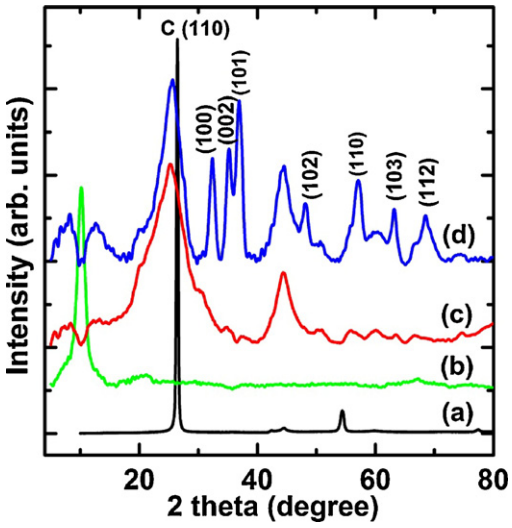

Fig. 3. XRD patterns for (a) graphite, (b) GO, (c) G-COOH, and (d) G-COOZn.

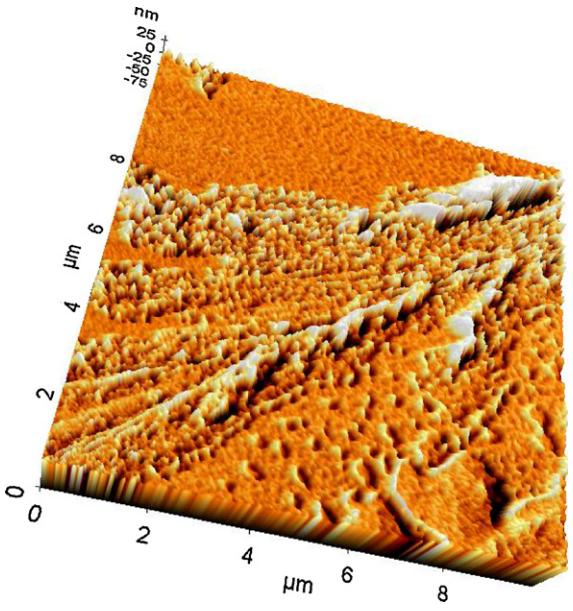

Fig. 4. Topography and height profile AFM images of G-COOZn.

47.4°, 56.6°, 62.8° and 68.5° originate from the (1 0 0), (0 0 2), (1 0 1), (1 0 2), (1 1 0), (1 0 3), and (1 1 2) reflections of ZnO.

AFM image (Fig. 4) provided morphological information about the G-COOZn. Sonication treatment of the G-COOZn reduced the size from several hundreds of nanometers to less than 10 μm in lateral width, while the thickness remained unaltered at ~10 nm (as revealed by the AFM images). On comparing this result with previous results in the literature [46,47], confirmed that the G-COOZn prepared in this work has the characteristics of a ZnO on G-COOH sheets.

Raman spectroscopy can be employed to characterize the bonding, ordering, and crystallite size in carbon materials. It is well known that the Raman band at around 1582 cm^{-1} (the G-band) is due to the in-plane phonon modes of graphene, which indicates sp^2 bonding. Also, the band at around 1353 cm^{-1} is due to disorder in the graphene layers caused by presence of sp^3 bonding (the D-band) [48]. Fig. 5 shows the Raman spectra of graphite, GO, G-COOH, and G-COOZn: the two peaks appearing at ca. 1350 and 1590 cm^{-1} correspond to the D and G bands, respectively. The Raman spectrum of graphite (Fig. 5(a)) shows the in-phase vibration of the graphite

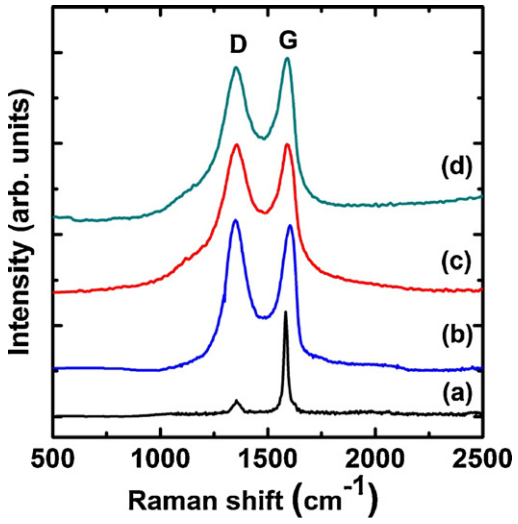

Fig. 5. Raman spectra of (a) graphite, (b) GO, (c) G-COOH, and (d) G-COOZn.

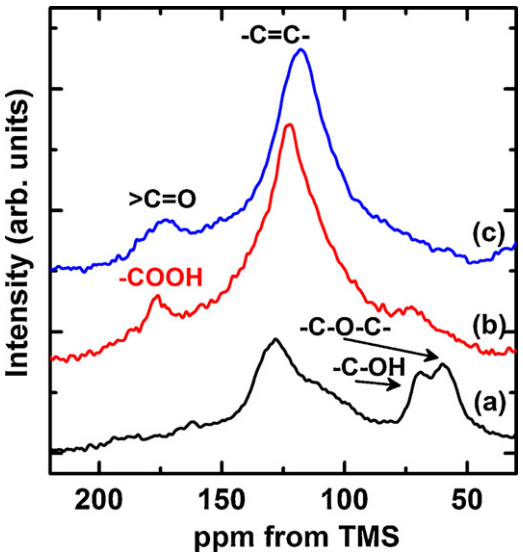

Fig. 6. ^{13}C-NMR spectra of (a) GO, (b) G-COOH, and (c) G-COOZn.

lattice at 1592 cm^{-1} (G band) and a weak D band at 1351 cm^{-1} [48,49], indicating its well-ordered structure. In the Raman spectrum of GO (Fig. 5(b)), the G band is broadened and shifts to higher frequency (1593 cm^{-1}) due to the presence of isolated double bonds that resonate at higher frequencies than the G band of graphite [50]. In addition, the D band at 1339 cm^{-1} becomes prominent, indicating the decrease in size of the in-plane sp^2 domains (G band) due to extensive oxidation during exfoliation. The Raman spectra of G-COOH and G-COOZn also exhibit D and G bands (Fig. 5(c) and (d)). Notably, the increase in the G/D intensity ratios for G-COOH and G-COOZn, compared to GO, indicates a decrease in the size of the in-plane sp^2 domains and, at the same time, an increase of those areas with disordered structure upon reduction [51].

The ^{13}C-NMR spectrum of GO (Fig. 6(a)) confirms the presence of abundant epoxide and hydroxyl groups [49,52], which one expected to align perpendicular to the basal-plane carbon atoms. The carboxyl groups, which are located at the edges of the basal plane, are too few for ^{13}C-NMR detection, in agreement with previous studies [49,52] on GO prepared by the Hummers' method [41]. After the reaction, however, the exfoliated GO (Fig. 6(b)) showed a significant reduction in the amount of epoxide and hydroxyl groups present. As seen in Fig. 6(c), the –COOH groups and the zinc ions in combination with the –COOZn generated, –COOH group disappeared. In addition, plentiful sp^2 carbon atoms were introduced, as shown by the increase in the peak height in the 90–150 ppm range, suggesting the formation of graphene-based materials.

The FT-IR spectra were obtained in order to characterize the oxygen-containing functional groups on the GO after reduction. Fig. 7(a) displays the characteristic peaks of the FT-IR spectra of GO: a broad band ranging from 3600 to 3250 cm^{-1} indicates the presence of –OH group, the stretching vibration for C=O from the carboxylic groups is at 1712 cm^{-1}, the stretching vibrations of C–O from the ether group occur at 1055 cm^{-1}, the in-plane –OH bending mode [53] at 1349 cm^{-1}, and the C=C aromatic ring stretching peak is present at 1570 cm^{-1}. From to the FT-IR spectra, it was confirmed that the GO contains the hydroxyl, carbonyl, carboxylic, and epoxy groups. After reaction of GO with chloroacetic acid and G-COOZn composites is shown in Fig. 7(b) and (c), the characteristic vibration bands due to $\nu_{C=O}$, ν_{C-O-C} and ν_{C-OH} vibrations decreased dramatically, indicating that efficient reduction of GO had occurred. New characteristic peaks at 457 cm^{-1} for the Zn–O stretching vibration of ZnO is now present.

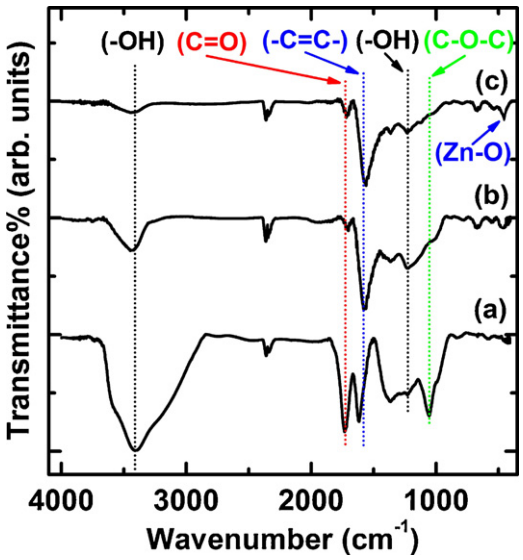

Fig. 7. FT-IR spectra of (a) GO, (b) G-COOH, and (c) G-COOZn.

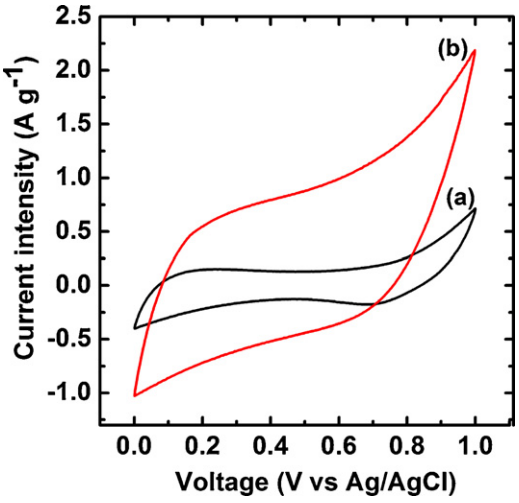

Fig. 9. CV curves of (a) G-COOH, and (b) G-COOZn.

The PL spectra were recorded without any post-preparative size separation. Typical PL spectra of G-COOH and G-COOZn at an excitation wavelength of 280 nm were shown in Fig. 8. Fig. 8(a) and (b) also shows the PL spectra of G-COOH at 364 nm, and G-COOZn at 369 and 382 nm. Due to the well-known quantum confinement effect, the PL peak positions located at 380 nm correspond to ZnO [54].

The performance of a supercapacitor device using the graphene based materials has been analyzed using CV, galvanostatic charge/discharge, and EIS. It is noted that EIS analysis has been recognized as one of the principal methods for examining the fundamental behavior of electrode materials for use in supercapacitors [55]. The specific capacitance is calculated from the slope of the charge–discharge curves [56]. The EIS data is analyzed using Nyquist plots. Each data point in the Nyquist plot is at a different frequency [56]. CV was considered to be a suitable tool for estimating the difference between the non-Faradic and Faradic reactions. CV curves obtained in a three-electrode cell for the G-COOH (Fig. 9(a)) and G-COOZn (Fig. 9(b)) electrodes at a voltage scan rate of 10 mV s^{-1} in 1 M Na_2SO_4 electrolyte using a Pt wire as the auxiliary electrode and Ag/AgCl as reference electrode are shown in Fig. 9. The CV curve of G-COOZn has a rectangular shape within a potential window of 0–1 V (vs Ag/AgCl), which has the characteristic of double layer capacitance. However, when the potential was increased to 0.9 V, the oxygen evolution became increasingly obvious.

Galvanostatic cycling of supercapacitor electrodes was performed at a constant current density of 50 mA g^{-1}. As seen in Fig. 10, the charge–discharge curves are linear in the total range of potential and have constant slopes, showing nearly perfect capacitive behavior [56–59]. The specific capacitance is evaluated from the slope of the charge–discharge curves, according to the equation $C = I\Delta t/(m\Delta V)$, where I is the applied current and m (21.0 mg, not including the mass of PEFE) is the mass of each electrode [53–56]. The maximum specific capacitance reaches ~238 F g^{-1}, and the maximum storage energy can be calculated as 119 Wh kg^{-1} from $CV_i^2/2$ [56,60], where C is the specific capacitance (238 F g^{-1}) and V_i is the initial voltage (1.0 V).

The charge–discharge curves for the G-COOZn at different specific currents (50, 30, and 10 mA g^{-1}) within the potential window of 0.0–1.0 V are shown in Fig. 11. Even at the high specific current of 50 mA g^{-1}, a specific capacitance of ~238 F g^{-1} is achieved, implying that the composite of G-COOH (0.5 g) to $Zn(NO_3)_2$ (1.00 g) ratio has a relatively good rate capability at specific current. Clearly it is

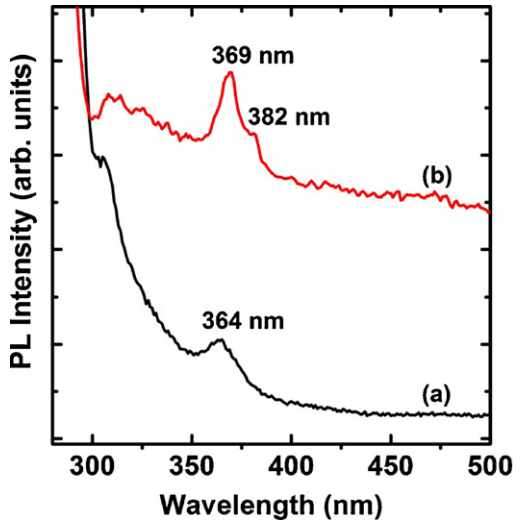

Fig. 8. PL spectra of (a) G-COOH, and (b) G-COOZn (excitation wavelength 280 nm).

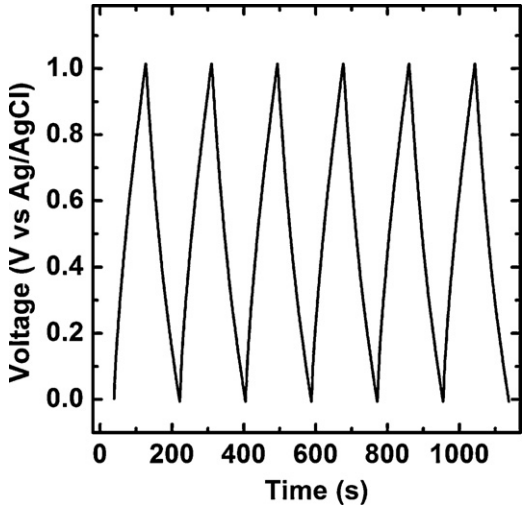

Fig. 10. Galvanostatic charge–discharge curves for G-COOZn at 50 mA g^{-1}.

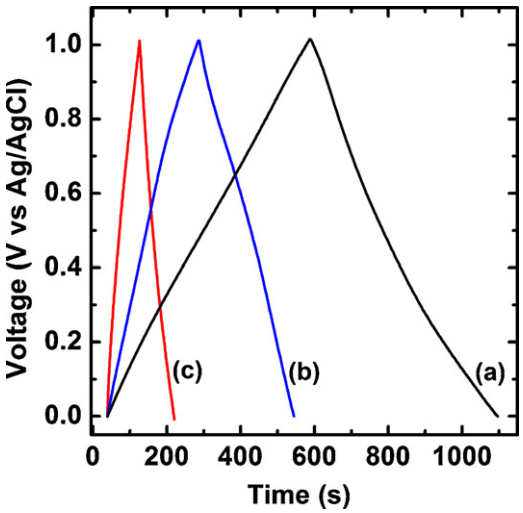

Fig. 11. Galvanostatic charge–discharge curves for G-COOZn at (a) 10 mA g^{-1}, (b) 30 mA g^{-1}, and (c) 50 mA g^{-1}.

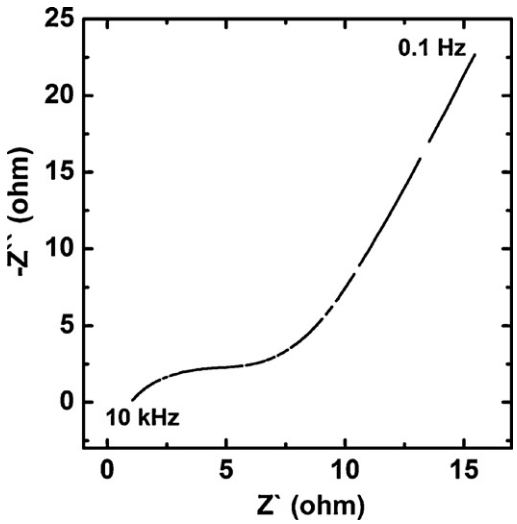

Fig. 13. Nyquist impedance plot of G-COOZn.

very important for the electrode materials of a supercapacitor to provide high power density.

Long cycling life is an important requirement for supercapacitor electrodes [61,56]. A cycling life test over 500 cycles for the ternary composite electrode was carried out. Fig. 12 demonstrates the very stable charge–discharge cycles obtained and also illustrates that the composites electrodes showed only less than 1% decay in available specific capacity after 500 cycles. The result of charge–discharge cycle testing of the ternary composite film suggests that the synergetic interaction between G-COOZn and PTFE significantly improved the electrical properties and the mechanical stability of the electrode.

A typical Nyquist impedance plots for this electrode is presented in Fig. 13; this was recorder under the following conditions: AC voltage amplitude of 50 mV and the frequency ranged from 0.1 Hz to 10 kHz at the initial potential of 0.1 V. The plot contains one depressed semicircle with larger diameter at high frequency due to high charge transfer resistance. The semicircular loop at high frequency is too small to identify and the slope of the impedance plot at low frequency increases and tends to become purely capacitive [62,63]. Meanwhile, the 45° sloped portion of the Nyquist impedance plot is attributed to the presence of Warburg resistance resulting from the frequency dependence of ion diffusion and transport in the electrolyte. The large Warburg region of these electrodes indicates the greater variations in ion diffusion path lengths and increased obstruction of ion movement.

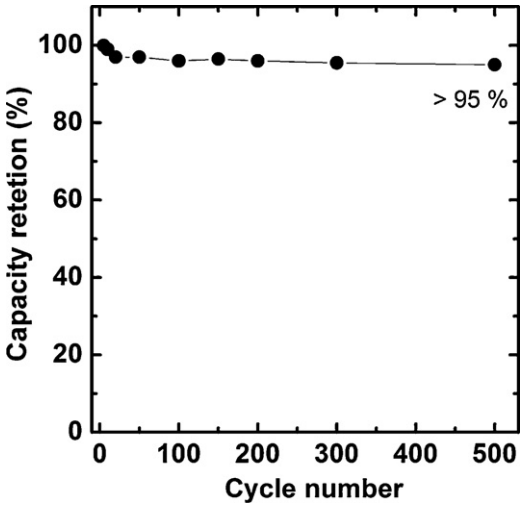

Fig. 12. Galvanostatic charge–discharge cycle test for G-COOZn at 50 mA g^{-1} (100% = ~238 F g^{-1}).

4. Conclusions

In summary, we have synthesized a G-COOZn composite employing a hydrothermal procedure and investigated its morphology and electrochemical performance. The composite achieves a specific capacitance as high as 238 F g^{-1} at 50 mA g^{-1} in the potential range of 0–1.0 V. While further detailed studies and optimization are required, from and present results we strongly believe that graphene-based materials show extremely strong potential for use in high efficiency supercapacitors.

Acknowledgments

This research was supported by WCU (World Class University) program (R32-2008-000-20003-0) through the National Research Foundation of Korea funded by the Ministry of Education, Science and Technology.

References

[1] J.D. Fowler, M.J. Allen, V.C. Tung, Y. Yang, R.B. Kaner, B.H. Weiller, ACS Nano 3 (2009) 301–306.
[2] W.J. Hong, Y.X. Xu, G.W. Lu, C. Li, G.Q. Shi, Electrochem. Commun. 10 (2008) 1555–1558.
[3] V.C. Tung, L.M. Chen, M.J. Allen, J.K. Wassei, K. Nelson, R.B. Kaner, Y. Yang, Nano Lett. 9 (2009) 1949–1955.
[4] L. Zhao, Y.X. Xu, T.F. Qiu, L.J. Zhi, G.Q. Shi, Electrochim. Acta 55 (2009) 491–497.
[5] M.H. Liang, L.J. Zhi, J. Mater. Chem. 19 (2009) 5871–5878.
[6] M.D. Stoller, S.J. Park, Y.W. Zhu, J.H. An, R.S. Ruoff, Nano Lett. 8 (2008) 3498–3502.
[7] Q. Wu, Y.X. Xu, Z.Y. Yao, A.R. Liu, G.Q. Shi, ACS Nano 4 (2010) 1963–1970.
[8] K.S. Novoselov, A.K. Geim, S.V. Morozov, D. Jiang, Y. Zhang, S.V. Dubonos, I.V. Grigorieva, A.A. Firsov, Science 306 (2004) 666–669.
[9] A.K. Geim, K.S. Novoselov, Nat. Mater. 6 (2007) 183–191.
[10] H.A. Becerril, J. Mao, Z.F. Liu, R.M. Stoltenberg, Z. Bao, Y.S. Chen, ACS Nano 2 (2008) 463–470.
[11] S. Stankovich, D.A. Dikin, R.D. Piner, K.A. Kohlhaas, A. Kleinhammes, Y. Jia, Y. Wu, S.T. Nguyen, R.S. Ruoff, Carbon 45 (2007) 1558–1565.
[12] S. Stankovich, D.A. Dikin, G.H.B. Dommett, K.M. Kohlhaas, E.J. Zimney, E.A. Stach, R.D. Piner, S.T. Nguyen, R.S. Ruoff, Nature 442 (2006) 282–286.
[13] D. Li, M.B. Müller, S. Gilje, R.B. Kaner, G.G. Wallace, Nat. Nanotechnol. 3 (2008) 101–105.
[14] S. Park, R.S. Ruoff, Nat. Nanotechnol. 4 (2009) 217–224.
[15] V.C. Tung, M.J. Allen, Y. Yang, R.B. Kaner, Nat. Nanotechnol. 4 (2009) 25–29.
[16] Z. Liu, J.T. Robinson, X. Sun, H.J. Dai, J. Am. Chem. Soc. 130 (2008) 10876–10877.

[17] J. Geng, H.T. Jung, J. Phys. Chem. C 114 (2010) 8227–8234.
[18] N. Karousis, A.S.D. Sandanayaka, T. Hasobe, S.P. Economopoulos, E. Sarantopoulou, N. Tagmatarchis, J. Mater. Chem. 21 (2011) 109–117.
[19] J.R. Lomeda, C.D. Doyle, D.V. Kosynkin, W.F. Hwang, J.M. Tour, J. Am. Chem. Soc. 130 (2008) 16201–16206.
[20] R. Muszynski, B. Seger, P.V.J. Kamat, J. Phys. Chem. C 112 (2008) 5263–5266.
[21] Y. Xu, Z. Liu, X. Zhang, Y. Wang, J. Tian, Y. Huang, Y. Ma, X. Zhang, Y. Chen, Adv. Mater. 21 (2009) 1275–1279.
[22] Y. Sui, J. Appenzeller, Nano Lett. 9 (2009) 2973–2977.
[23] C.S. Shan, H.F. Yang, J.F. Song, D.X. Han, A. Ivaska, L. Niu, Anal. Chem. 81 (2009) 2378–2382.
[24] D.W. Wang, F. Li, J.P. Zhao, W.C. Ren, Z.G. Chen, J. Tan, Z.S. Wu, I. Gentle, G.Q. Lu, H.M. Cheng, ACS Nano 3 (2009) 1745–1752.
[25] P. Guo, H.H. Song, X.H. Chen, Electrochem. Commun. 11 (2009) 1320–1324.
[26] Y. Wang, Z.Q. Shi, Y. Huang, Y.F. Ma, C.Y. Wang, M.M. Chen, Y.S. Chen, J. Phys. Chem. C 113 (2009) 13103–13107.
[27] Y.P. Zhang, H.B. Li, L.k. Pan, T. Lu, Z. Sun, J. Electroanal. Chem. 634 (2009) 68–71.
[28] B.J. Lee, S.R. Sivakkumar, J.M. Ko, J.H. Kim, S.M. Jo, D.Y. Kim, J. Power Sources 168 (2007) 546–552.
[29] Y. Shan, L. Gao, Mater. Chem. Phys. 103 (2007) 206–210.
[30] G. Arabale, D. Wagh, M. Kulkarni, I.S. Mulla, S.P. Vernekar, K. Vijayamohanan, A.M. Rao, Chem. Phys. Lett. 376 (2003) 207–213.
[31] P.X. Gao, Z.L. Wang, Small 1 (2005) 945–949.
[32] D. Kalpana, K.S. Omkumar, S.S. Kumar, N.G. Renganathan, Electrochim. Acta 52 (2006) 1309–1315.
[33] M. Jayalakshmi, K. Balasubramanian, Int. J. Electrochem. Sci. 3 (2008) 1196–1217.
[34] Y.L. Chen, Z.A. Hu, Y.Q. Chang, H.W. Wang, Z.Y. Zhang, Y.Y. Yang, H.Y. Wu, J. Phys. Chem. C 115 (2011) 2563–2571.
[35] W.T. Zheng, Y.M. Ho, H.W. Tian, M. Wen, J.L. Qi, Y.A. Li, J. Phys. Chem. C 113 (2009) 9164–9168.
[36] H. Li, M. Eddaoudi, M. O'Keeffe, O.M. Yaghi, Nature 402 (1999) 276–279.
[37] W. Yuan, T. Friščić, D. Apperley, S.L. James, Angew. Chem. Int. Ed. 49 (2010) 3916–3919.
[38] R. Zou, A.I. Abdel-Fattah, H. Xu, Y. Zhaob, D.D. Hickmotta, Crystallogr. Eng. Commun. 12 (2010) 1337–1353.
[39] X. Sun, Z. Liu, K. Welsher, J.T. Robinson, A. Goodwin, S. Zaric, H. Dai, Nano Res. 1 (2008) 203–212.
[40] G.T. Hermanson, Bioconjugate Techniques, Academic Press, San Diego, 1996 (Chapter 2).
[41] W. Hummers, R. Offeman, J. Am. Chem. Soc. 80 (1958) 1339.
[42] S. Donner, H.W. Li, E.S. Yeung, M.D. Porter, Anal. Chem. 78 (2006) 2816–2822.
[43] H.K. Jeong, Y.P. Lee, R.J.W.E. Lahaye, M.H. Park, K.H. An, I.J. Kim, C.W. Yang, C.Y. Park, R.S. Ruoff, Y.H. Lee, J. Am. Chem. Soc. 130 (2008) 1362–1366.
[44] C. Xu, X. Wang, J. Zhu, J. Phys. Chem. C 112 (2008) 19841–19845.
[45] A.B. Bourlinos, D. Gournis, D. Petridis, T. Szabo, A. Szeri, I. Dekany, Langmuir 19 (2003) 6050–6055.
[46] H. Wang, L. Wang, C. Qu, Y. Su, S. Yu, W. Zheng, Y. Liu, J. Solid State Chem. 184 (2011) 881–887.
[47] G. Williams, P.V. Kamat, Langmuir 25 (2009) 13869–13873.
[48] F. Tuinstra, J.L. Koenig, J. Chem. Phys. 53 (1970) 1126–1130.
[49] A.C. Ferrari, J.C. Meyer, V. Scardaci, C. Casiraghi, M. Lazzeri, F. Mauri, S. Piscanec, D. Jiang, K.S. Novoselov, S. Roth, Phys. Rev. Lett. 97 (2006) 187401–187404.
[50] K.N. Kudin, B. Ozbas, H.C. Schniepp, R.K. Prud'homme, I.A. Aksay, R. Car, Nano Lett. 8 (2008) 36–41.
[51] A.C. Ferrari, J. Robertson, J. Phys. Rev. B 61 (2000) 14095–14107.
[52] A. Lerf, H.Y. He, M. Forster, J. Klinowski, J. Phys. Chem. B 102 (1998) 4477–4482.
[53] L.J. Bellamy, The Infrared Spectra of Complex Molecules, Chapman and Hall, London, 1975.
[54] V.A. Fonoberov, K.A. Alim, A.A. Balandin, Phys. Rev. B 73 (2006) 165317–165319.
[55] W. Sugimoto, H. Iwata, K. Yokoshima, Y. Murakami, Y. Takasu, J. Phys. Chem. B 109 (2005) 7330–7738.
[56] B.E. Conway, Kluwer Academic/Plenum Publishers, New York, 1999 (Chapter 15).
[57] D.Y. Qu, J. Power Sources 109 (2002) 403–411.
[58] A. Burke, J. Power Sources 91 (2000) 37–50.
[59] A. Nishino, J. Power Sources 60 (1996) 137–147.
[60] E. Raymundo-Piñero, F. Leroux, F. Béguin, Adv. Mater. 18 (2006) 1877–1882.
[61] P. Simon, Y. Gogotsi, Nat. Mater. 7 (2008) 845–854.
[62] L. Cao, F. Xu, Y.Y. Liang, H.L. Li, Adv. Mater. 20 (2004) 1853–1857.
[63] Q.F. Wu, K.X. He, H.Y. Mi, X.G. Zhang, Mater. Chem. Phys. 101 (2007) 367–371.